Individual vaccine efficacy variation with time since mRNA BNT162b2 vaccination estimated by rapid, quantitative antibody measurements from a finger-prick sample.

Matheus J. T. Vargas [a], Mithileshwari Chandrasekhar [a], Yong Je Kwon [a] Gerrit Sjoerd Deijs [a], Carsten Ma On Wong Corazza [a], Angela (Wai Yin) Chai [a], Rebecca L. Binedell [a], Ellen Jose [a], Bhavesh Govind [a], Laura Huyet [a], Pooja K. Patel [a], Gabrielle Reshef [a], Vijaya Kumar [a], Tiffany Lowe [a], Robert J. Powell [b], Kieran C. Jina [a], Flynn C.W. Walker [a], Apisalome Talemaitoga, MD [c], M. Cather Simpson [d], David E. Williams*[,d]

a. Orbis Diagnostics Ltd, 125 Queen Street, Auckland 1010, New Zealand
b. Pacific Channel Ltd, PO Box 106 818, Auckland 1143, New Zealand
c. Cavendish Clinic, 175 Cavendish Drive, Manukau, Auckland, New Zealand
d. School of Chemical Sciences, University of Auckland, Private Bag 92019, Auckland 1142, New Zealand

Corresponding Author. Email: david.williams@auckland.ac.nz

Abstract

We show that an individual's immune status to Covid-19 can be monitored through quantitative antibody measurements using a method specifically designed for high throughput and accuracy from a finger-prick blood sample. The quality of the rapid test results is comparable to that from major commercial laboratory testing kits. Anti-Receptor Binding Domain (RBD) IgG concentration showed a log-normal distribution with mean decreasing with time following the second vaccination with mRNA BNT162b2 (Pfizer). Using a model for an individual's antibody concentration-dependent vaccine efficacy allowed comparison with literature data on changing vaccine efficacy against symptomatic disease across a population. In this small trial (n = 100) estimated median vaccine efficacy was 90% (range 65-95%) < 90 days post vaccination, 75% (range 35 – 90%) 90 – 170 days and 65% (range 35-90%) 170 – 230 days. The results provide strong support for personalized booster programmes that, by targeting people in the tail of the distribution, should be more effective at diminishing breakthrough infection and optimising booster dose supply than a program that simply mandates a booster at a specific post-vaccination time point.

Introduction

The Orbis high-throughput quantitative immunity measurement system implements an enzyme-linked immunosorbent assay adapted for accurate, precise, rapid-testing (<20 min) on a centrifugal microfluidic platform. All operations post sample collection and loading onto the instrument are automated. The sample is a small drop of whole blood obtained from a finger-prick. The assay is designed for speed – multiple samples are measured at the same time with a total assay time less than 20 min – and for accuracy. The important elements of the assay design are rapid, complete mixing and accurate timing. These features mean that a kinetically-controlled assay can be implemented: concentration is deduced from the rate of binding ('on' rate) of the target to the capture surface; a wide, linear dynamic range is achieved. The capture surface is a single small bead that carries the SARS-CoV-2 – Receptor Binding Domain (RBD) protein so the measurement is of IgG concentration directed at this key protein. Speed of mixing is obtained by rapid oscillation of the disc motion to cause oscillation of the bead within the chamber, whose shape is also controlled to promote mixing [1]. The assay performs with high analytical sensitivity, therefore samples are diluted

in the machine with 10x addition of buffer. The buffer dilution step also minimises effects of non-specific adsorption of blood components. The details of the assay design and results on buffer solutions are given in Supplementary Appendix 1, demonstrating repeatability of duplicate measurements of 10% across a range of 5 – 500 ng/mL of IgG.

As part of the device development, a small clinical trial was conducted [2]. The primary outcome was to demonstrate the system's ability to distinguish fully vaccinated from unvaccinated people by means of a simple and rapid procedure, that might for example be used for entry control or validation of a vaccine passport: an approach of intense current interest. Vaccinated participants had a range of age and time since completion of vaccination (2 doses separated by at least 3 weeks). Because of the nature of the primary outcome, there was no selection by age, date since vaccination, ethnicity or socio-economic factors. Participant age and time since vaccination were recorded as was the experience of the participants and sampling system operators during the process of taking the sample. The resulting data provided a distribution across the sample of anti-SARS-CoV-2 – RBD IgG concentration. This paper presents the results of an analysis of the change in antibody concentration distribution with time since vaccination.

Results

The output of the measurement is the concentration of anti-RBD IgG with respect to a buffer control that is measured simultaneously. Assay validation used buffer controls and the panel of samples provided by the National Institute of Biological Standards and Controls, UK, NIBSC 20/B770. This panel contains as a package insert the results of analyses using a number of different assay platforms. The Orbis assay result was converted to Binding Antibody Units (BAU) for the RBD using WHO and NIBSC standards NIBSC 20/162, 20/150, 20/148 20/144 and 20/140. Correlation of Orbis assay results with the standards, comparison of results for different assay platforms using the data provided with NIBS 20/B770, and comparison of Orbis assay results with the data provided with NIBS 20/B770 is given in Supplementary Appendix 2. There is a significant scatter of results across the different platforms. These results show that the Orbis assay gives results that are very comparable with a number of commercial assay platforms.

The distribution of anti-RBD IgG concentrations for vaccinated and unvaccinated participants is shown in Supplementary Fig 1. The results for vaccinated participants showed a log-normal distribution of concentration. Unvaccinated participants also showed a signal, but this was significantly smaller and normally distributed. Antigen (RBD) titration and measurement using buffers containing fibrinogen showed that this result was due to non-specific adsorption of the secondary indicator antibody promoted by fibrinogen adsorption to the assay chamber walls and it can therefore be treated as a normally distributed offset error. In the following, the mean value from this background effect has been subtracted from the assay results for vaccinated participants.,

Participant age was fairly uniformly distributed across the range 20 – 60 yr. The vaccination date correlated data fall into 3 clearly distinguishable ranges (fig 1 inset): < 90 days, 90 – 170 days and 170 – 228 days. Figure 1 shows the empirical cumulative probability distribution of anti-RBD IgG concentration for these 3 ranges. Figure 1 also shows the fit to a log-normal distribution. The log-normal mean decreases with time since vaccination (Table 1). The effect is highly significant (<0.5% for the Kolmogorov-Smirnov test) between < 90 days and 90 – 170 days, and marginally significant (10% K-S) between 90 – 170 days and 170 – 228 days. An effect of age correlated with time since vaccination was marginally discernable in the data but without statistical significance. Thus the following discussion focusses on the effect of time since vaccination.

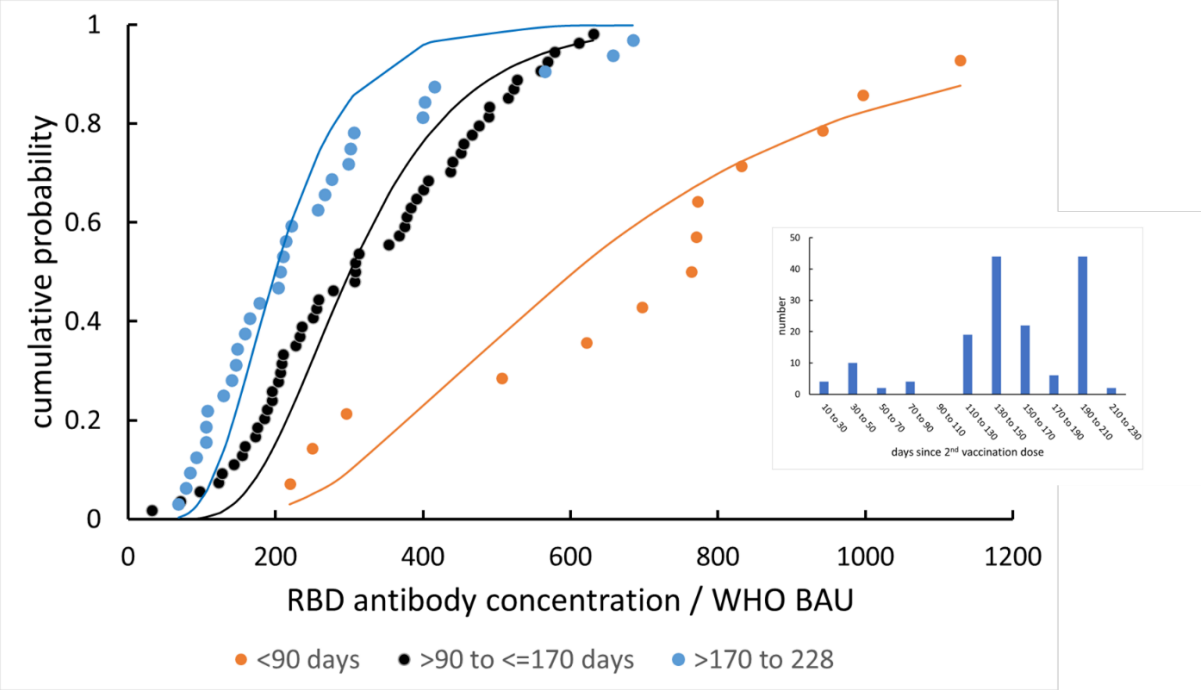

Figure 1. Anti-RBD IgG concentration distribution (offset subtracted), and its alteration with time since vaccination. The lines are fits to a log-normal distribution. Inset: distribution of vaccination dates across the study participants.

Discussion and Implications

Vaccine efficacy against symptomatic illness is now clearly known to decay with time following completion of vaccination, significantly over the first 6 months [3, 4]. The large study by Tartof et al.[3] provides good information about the breakthrough infection probability for a population, expressed as vaccine efficacy, VE, as a function of time following vaccination. Given the antibody concentration distribution shown in Figure 1, assuming that the probability of symptomatic infection is determined by the binding of IgG to the RBD [5] and using a model relating symptomatic infection probability to the anti-RBD concentration [5, 6], the population breakthrough infection probability and hence population VE can be calculated from the data collected in the study reported here. Estimation of the model parameters to match the calculated population VE with that observed by Tartof et al. allows calculation of an estimate of individual VE given the individual anti-RBD concentration. The detail of the calculation is given in Supplementary Appendix 3. Briefly, the model [5, 6] is:

$$E_I(c) = 1/[1 + (c_{50}/c)^k] \quad (1)$$

where $E_I(c)$ denotes individual vaccine protective efficacy as a function of concentration, c, of anti RBD IgG. The curve is a sigmoidal variation of ln(c). The parameters are c_{50} and k where c_{50} denotes the concentration for 50% vaccine efficacy and k controls the rate of increase of efficacy with concentration around c_{50} . The population VE is calculated by integration over the population distribution of antibody concentration. The aim is to find a set of parameters that is not only consistent with the population VE for different date ranges, but also consistent with the observed antibody concentration distribution across the different date ranges and with model constraints on c_{50} and k [5-7]. Figure 2 shows the results and Table 1 lists the parameters and compares the observed

and calculated population VE. The limitation of this study is that the small number of participants, without comprehensive coverage of the full range of vaccination date, meant that the full range of breakthrough infection rate data dependent on vaccination date could not be used. The probability distribution of concentration for the full range of date also could not be assessed accurately: specifically, to have sufficient data in each date range, the date ranges were broad and thus there was not a strong discrimination between the results for the later date ranges. Both these limitations led to uncertainty in the assessment of the distribution of individual vaccine efficacy. Despite these limitations, the effect of time since vaccination on individual vaccine efficacy distribution is clear and the model has captured the general trend well.

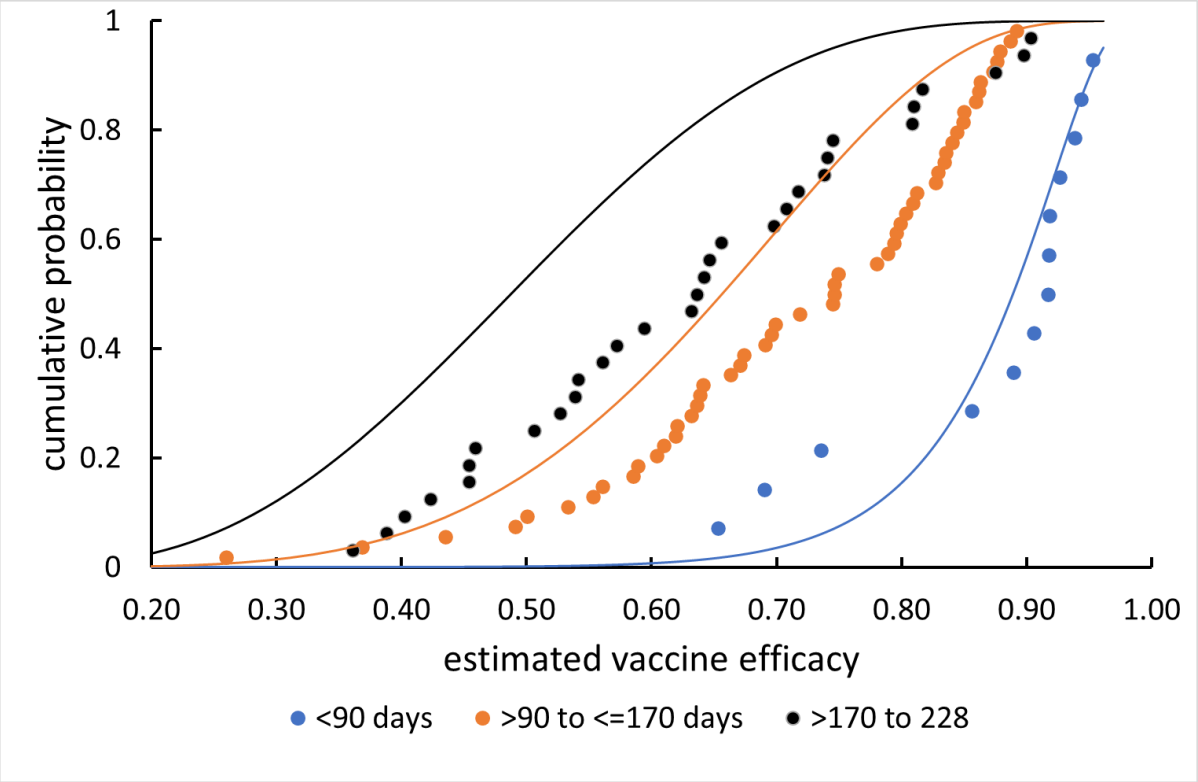

Figure 2. Empirical cumulative probability distribution of vaccine efficacy across different ranges of time since vaccination, estimated using the data of Tartof et al [3], the concentration distributions shown in Figure 1 and the calculation given in Supplementary Appendix 3. The lines are the fitted theoretical distributions.

Time range / days	< 90	90 - 170	170 - 228
μ	1.62	0.78	0.39
σ	0.4		
Population VE(observed: Tartof)/ %	83	64	47
Population VE(calculated)	82	64	49
c_{50} / BAU	206		
k	1.70		

Table 1. Observed and calculated population vaccine efficacy. The parameters for the (natural) log-normal concentration distributions are μ and σ. As described in Supplementary Appendix 3, the fit has been constrained with σ the same for all time ranges. The derived parameters c_{50} and k are consistent with previous studies[5-7] .

Figure 2 illustrates the very significant range of estimated VE across the participants in this study. The effect of the log-normal distribution of concentration is that the most significant contribution to breakthrough infections comes from people in the low-concentration tail of the distribution. From Figure 2, estimated median vaccine efficacy 90% (range 65-95%) < 90 days post vaccination, 75% (range 35 – 90%) 90 – 170 days and 65% (range 35-90%) 170 – 230 days though the theoretical model implies that the range at longer time may be significantly larger. The results have implications for the design of booster vaccination programmes directed at optimising the use of booster doses in order to achieve the best possible population protection. Since the most significant contribution to breakthrough infections comes from people in the low-concentration tail of the distribution, it is arguable that any booster programme should be directed at these. It would arguably be less useful to boost those in the high concentration tail. Significant numbers of people can be found in the low-concentration tail relatively recently after completion of vaccination whilst others can be found in the high concentration tail even after 6 months. Therefore a vaccination programme that simply targets all people > 6 months after vaccination, whilst administratively convenient, will miss an important proportion of the population at risk and will also unnecessarily boost others. There is now a focus on quantitative antibody tests that promote an increased understanding of immune responses to SARS-CoV-2 [8]. The work described here has demonstrated a fast and accurate, point-of-need, finger-prick immunoassay method that overcomes the well-known limitations of lateral-flow rapid assay methods and is appropriate for large-scale studies. Despite the limitations imposed by the small sample size, particularly the lack of resolution in date range over a full 6 months leading to uncertainty in model parameter estimation, the work has demonstrated that a rapid antibody measurement can build the evidence needed to construct the targeted booster programmes that are now being called for [9].

Acknowledgement

DEW acknowledges early support through an E.T.S Walton Visiting Fellowship of Science Foundation Ireland. The work has been funded by Orbis Diagnostics. We thank the staff of Cavendish Clinic, Manukau, Auckland for their management, sample collection and interaction with the participants for the clinical trial, and particularly thank the participants themselves. The prototype instrument used for this trial was designed and constructed by D&K Engineering, San Diego, California; particular thanks to David Kortbawi, Sean McCrossin, Victor Escobedo, Don Fox and John Muren.

Conflict of Interest

MCS and KCJ are Directors of Orbis Diagnostic Ltd. Other than AT, authors are shareholders and/or employees of Orbis Diagnostics Ltd or its lead investor, Pacific Channel.

References

1. Simpson, M. C.; Vargas, M. J. T.; Chandrasekhas, M.; Williams, D. E. Multi-chambered assay devices and associated methods, systems and apparatuses thereof for detection of analytes. International Patent Cooperation Treaty application WO 2021/189054 A1. 2021.
2. A Phase I, Single-Site study to Test the Sensitivity and Specificity of the Orbis Quantitative Immunity for COVID-19 (QIC) Test in Detecting Levels of Anti-SARS-CoV2 IgG Antibodies in Vaccinated and Un-Vaccinated Airline Staff, Universal Trial Number U1111-1267-3749 , https://www.anzctr.org.au/Trial/Registration/TrialReview.aspx?id=382309&isReview=true.
3. Tartof, S. Y.; Slezak, J. M.; Fischer, H.; Hong, V.; Ackerson, B. K.; Ranasinghe, O. N.; Frankland, T. B.; Ogun, O. A.; Zamparo, J. M.; Gray, S.; Valluri, S. R.; Pan, K.; Angulo, F. J.; Jodar, L.; McLaughlin, J. M., Effectiveness of mRNA BNT162b2 COVID-19 vaccine up to 6 months in a large

integrated health system in the USA: a retrospective cohort study. *The Lancet* **2021,** *398* (10309), 1407-1416.

4. Mizrahi, B.; Lotan, R.; Kalkstein, N.; Peretz, A.; Perez, G.; Ben-Tov, A.; Chodick, G.; Gazit, S.; Patalon, T., Correlation of SARS-CoV-2 Breakthrough Infections to Time-from-vaccine; Preliminary Study. *medRxiv* **2021**, 2021.07.29.21261317.

5. Williams, D. E., COVID 19 breakthrough infection risk: a simple physical model describing the dependence on antibody concentration. *bioRxiv* **2021**, 2021.10.25.465798.

6. Khoury, D. S.; Cromer, D.; Reynaldi, A.; Schlub, T. E.; Wheatley, A. K.; Juno, J. A.; Subbarao, K.; Kent, S. J.; Triccas, J. A.; Davenport, M. P., Neutralizing antibody levels are highly predictive of immune protection from symptomatic SARS-CoV-2 infection. *Nature Medicine* **2021,** *27* (7), 1205-1211.

7. Wall, E. C.; Wu, M.; Harvey, R.; Kelly, G.; Warchal, S.; Sawyer, C.; Daniels, R.; Hobson, P.; Hatipoglu, E.; Ngai, Y.; Hussain, S.; Nicod, J.; Goldstone, R.; Ambrose, K.; Hindmarsh, S.; Beale, R.; Riddell, A.; Gamblin, S.; Howell, M.; Kassiotis, G.; Libri, V.; Williams, B.; Swanton, C.; Gandhi, S.; Bauer, D. L. V., Neutralising antibody activity against SARS-CoV-2 VOCs B.1.617.2 and B.1.351 by BNT162b2 vaccination. *Lancet* **2021,** *397* (10292), 2331-2333.

8. Food and Drug Administration, USA: Policy for Coronavirus Disease-2019 Tests During the Public Health Emergency (Revised): : https://www.fda.gov/media/135659/download (accessed 30 November 2021).

9. World Health Organisation: Interim statement on booster doses for COVID-19 vaccination https://www.who.int/news/item/04-10-2021-interim-statement-on-booster-doses-for-covid-19-vaccination. (accessed 30 November 2021).

Supplementary Appendix 1

Individual vaccine efficacy variation with time since mRNA BNT162b2 vaccination estimated by rapid, quantitative antibody measurements from a finger-prick sample.

Matheus J. T. Vargas, Mithileshwari Chandrasekhar, Yong Je Kwon, Gerrit Sjoerd Deijs, Carsten Ma On Wong Corazza, Angela (Wai Yin) Chai, Rebecca L. Binedell, Ellen Jose, Bhavesh Govind, Laura Huyet, Pooja K. Patel, Gabrielle Reshef, Vijaya Kumar, Tiffany Lowe, Flynn C.W. Walker, Apisalome Talemaitoga, MD, M. Cather Simpson, David E. Williams*

Assay design

1. Assay principles: comparison of titration (equilibrium of target with capture sites) with kinetic (binding rate of target to capture sites)-determined assays
    a. Orbis assay is a kinetic assay
2. Kinetic assay model
    a. Primary binding step
    b. Secondary binding step
3. Model results
    a. Effect of varying primary incubation time
    b. Effect of varying secondary incubation time
    c. Effect of varying secondary concentration
    d. Effect of varying wash time
4. Signal generation
    a. Expected time-dependence of assay signal
    b. Confirmation of expected time dependence of signal
    c. Confirmation of expected dependence of rate constant for signal generation on target concentration and demonstration of high sensitivity and wide dynamic range

1. Assay principles

Immunoassay of the 'sandwich' or 'indirect ELISA' type comprises the following steps:

(a) Primary binding step - Mixing of the sample with a surface that has binding sites specific for the target analyte (eg a surface carrying bound antigen to a target antibody). The target binds to sites on the surface. After some time, the reaction is stopped and any unbound material is washed away.
(b) Incubation of the surface carrying the captured target with a label that binds only onto captured target. After some time the reaction is stopped and any unbound material is washed away. The amount of label remaining on the surface is measured, thus giving the amount of captured target and hence the original sample concentration.

There are two contrasting methods for the primary binding step, for connecting the solution concentration to the amount of captured analyte:

(a) The primary binding step is run for a time sufficiently long that the surface reaches equilibrium with the solution (titration method)

(b) The primary binding step is run for a short time: the amount captured is determined by the kinetics of reaction of the analyte with the surface. For an accurate determination, this method requires precise control of mixing, which should be very rapid in comparison with the time scale of the reaction (determines time zero and concentration uniformity during the reaction) and precise control of reaction time.

The determining time scale for an antibody-antigen reaction is the 'off' rate: the rate of dissociation of antibody from antigen (typically 10^{-3} s^{-1}) . For the equilibrium titration method, the time for the primary binding step needs to be several times the reciprocal of the 'off' rate: so at least 1 hr. For the kinetic method, the time scale for the primary binding step can be short in comparison with the reciprocal of the 'off' rate. Because the surface-bound antibody-antigen complex can dissociate during the washing and secondary binding steps, the time scale for these steps should be short in comparison with the reciprocal of the 'off' rate, and well-controlled.

The Orbis assay is a kinetic assay. The key is rapid and complete mixing upon addition of both the sample and the label to the capture surface, and precise timing of each step. The following sections develop the theoretical model for this type of assay.

2. Kinetic assay model

The capture surface has a total number, N_A, of capture sites available. These sites are assumed sufficiently widely spaced that they are independent of one another – there is no interaction between sites that alters the probability of reaction of a given site dependent on the occupation of neighbouring sites. At any time ,t, following the start of the reaction, a fraction, θ, of these sites are occupied by analyte. Hence the number of empty sites at time, t, is $(1-\theta)N_A$. The analyte has solution concentration, c, with value c_0 at the start of the reaction (t = 0); c_0 is the quantity to be determined by the assay procedure. The rate constant for attachment of analyte is k_{on} and for detachment is k_{off} .

The treatment below assumes that the number of binding sites is sufficiently large that there is no need to develop a stochastic model (that is, to count the binding events as discrete steps, one molecule at a time). A continuum model is given.

Primary binding step: For the primary binding step:

$$\frac{d\theta}{dt} = k_{on}c(1-\theta) - k_{off}\theta \tag{1}$$

The total amount of analyte, bound and free, is fixed, so:

$$c_0 = c + \frac{\theta N_A}{V} \tag{2}$$

$$\frac{d\theta}{dt} = \left[k_{on}\left(c_0 - \frac{\theta N_A}{V}\right)(1-\theta)\right] - k_{off}\theta \tag{3}$$

The initial state, at t = 0, is θ = 0. At the end of the primary binding step, at $t = t_{prim}$, the amount bound will be $\theta_1 N_A$, which is to be computed by integration of equation (3).

First washing step: During the first washing step, analyte will dissociate from the surface.

$$\frac{d\theta}{dt} = -k_{off}\theta \tag{4}$$

The initial state, at $t = 0$, is $\theta = \theta_{1,t = tprim}$. After time $t = t_{wash}$, the amount remaining will be $\theta_{2,0}$, the starting condition for the next step,which is computed by integration of equation (4):

$$\theta_{2,0} = \theta_{1,t=t_{prim}} \exp\left(-k_{off} t_{wash}\right) \tag{5}$$

Secondary binding step: The secondary binding step is described in the same way as the first, with initial secondary reagent concentration $c_{sec,0}$, and with reaction rate constants $k_{on,sec}$ and $k_{off,sec}$. The binding is to sites on the surface that have target analyte bound following the primary binding step and the first wash. Two processes are happening. First, the target analyte continues to dissociate from the surface, so the available number of binding sites decreases with time. Since the amount bound is small, the concentration resulting in solution will be small and is assumed to be zero. Second, the secondary (indicator) reagent will be binding to those primary molecules that remain on the surface. It will also be dissociating as will the target to which it is bound :

$$\frac{d\theta_2}{dt} = \left[k_{on,sec}\left(c_{sec,0} - \frac{\theta_2 N_A}{V}\right)\left(\theta_{2,0} - \theta_2\right)\right] - k_{off,sec}\theta_2$$

And the target is also dissociating from both sites carrying indicator and those which are not

$$\frac{d\theta_{2,0}}{dt} = -k_{off}\theta_{2,0} \tag{6}$$

If the secondary reagent concentration is sufficiently high, then the amount bound can be ignored in relation to the amount present in solution, in which case:

$$\frac{d\theta_2}{dt} = \left[k_{on,sec} c_{sec,0}\left(\theta_{2,0} - \theta_2\right)\right] - k_{off,sec}\theta_2 - k_{off}\theta_2 \tag{6a}$$

The initial state, at $t = 0$, is $\theta = \theta_{2,0}$. At the end of the secondary binding step, at $t = t_{sec}$, the amount bound will be $(\theta_3 N_A)_{t = tsec}$, which is the initial state for the next step and which is to be computed by integration of equation (6).

Second wash step . During the second wash step, time t_{wash} , the indicator reagent can be lost both by dissociation of the indicator-analyte complex and by dissociation of the analyte from the surface.

$$\frac{d\theta_2}{dt} = -\left(k_{off} + k_{off,sec}\right)\theta_2 \tag{7}$$

The amount remaining after the wash time would be

$$\theta_{2,final}N_A = (\theta_3 N_A)_{t=t_{sec}} \exp\left(-\left(k_{off} + k_{off,sec}\right)t_{wash}\right) \tag{8}$$

This is the amount that is measured when the indicator is measured and is therefore the assay result.

The parameters that can be controlled to tune the assay result are the number of binding sites on the capture surface, N_A , the times t_{prim} , t_{sec} , and t_{wash} , and the concentration of the secondary (indicator) reagent, $c_{sec,0}$.

3. *Model results*

The equations are solved numerically. For the purpose of modelling the behaviour it is reasonable to assume that the binding and dissociation rate constants for the primary and secondary steps are so similar that they can be taken to be the same. This conveniently reduces the number of variable parameters and simplifies the scaling needed for numerical solution.

Time and concentration are scaled to be dimensionless. Time is taken as the ratio to the 'on' time, $\tau = V/(k_{on}N_A)$. and concentration to N_A/V which is the 'concentration' of binding sites in relation to the solution volume. Denoting the scaled time by T and concentration by Γ:

Primary binding:

$$\frac{d\theta}{dT} = (\Gamma - \theta)(1 - \theta) - K_{off}\theta \tag{9}$$

First wash:

$$\theta_{2,0} = \theta_{1,T=T_{prim}} \exp\left(-K_{off}T_{wash}\right) \tag{10}$$

Secondary binding:

$$\frac{d\theta_2}{dT} = \Gamma_{sec}\left(\theta_{2,0} - \theta_2\right) - K_{off}\theta_2$$

$$\frac{d\theta_{2,0}}{dT} = -K_{off}\theta_{2,0} \tag{11}$$

Secondary wash:

$$\theta_{2,final} = \theta_{2,T=T_{sec}} \exp\left(-2K_{off}T_{wash}\right) \tag{12}$$

The final result is the dependence of $\theta_{2,final}$ on Γ, with the variable parameters Γ_{sec} , T_{prim} , T_{sec} , and T_{wash}

Figure 1 shows the time-variation of coverage of captured analyte in the primary binding step. At longer time, the signal saturates: this is the regime for an equilibrium assay. At sufficiently short time, the increase of coverage is linear with time and at fixed time is linear in concentration. This is the regime for a kinetically-controlled assay. In this regime, the precision of the assay result will be determined by the precision with which time zero is known – hence the need for rapid and efficient mixing of the sample solution with the capture surface – and by the precision of timing the end of the primary incubation step- hence precision and speed in flushing the sample solution away from the surface, fast introduction of the wash and rapid and efficient mixing in the wash step. Figure 2 shows the time variation of the coverage of the secondary indicator, with varying secondary reagent concentration, for a particular target analyte concentration, primary incubation time, washing time and dissociation rate constant. The dissociation of the indicator off the capture surface can be an important issue and there is an interaction between the effects of secondary incubation time and secondary reagent concentration. For a reliable assay system, ideally the result should be independent of the secondary reagent concentration. Figure 2 shows that this can be achieved if the secondary reagent concentration is high enough and the incubation time is long enough. Longer incubation leads to loss of signal but higher secondary reagent concentration could lead to issues of non-specific binding of this reagent which would then lead to erroneously high assay results. The effect of dissociation is to impose strong requirements on the precision of timing for both the wash and secondary incubation steps.

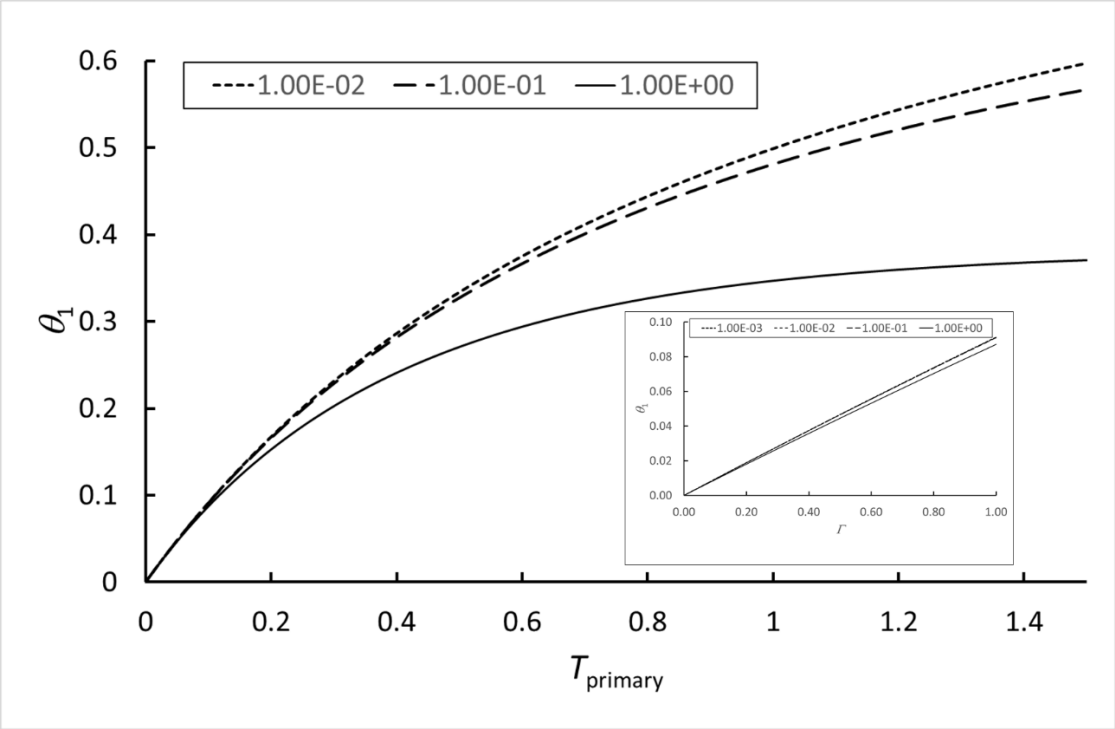

Figure 1 Variation of surface coverage of analyte captured during the primary binding step, θ_1, with time, $T = tk_{on}N_A/V$ Inset: variation of θ_1 at $T_{primary} = 0.1$ with scaled analyte concentration, $\Gamma = c_0V / N_A$. Parameter: "off" rate, $K_{off} = k_{0ff}V/k_{on}N_A$.

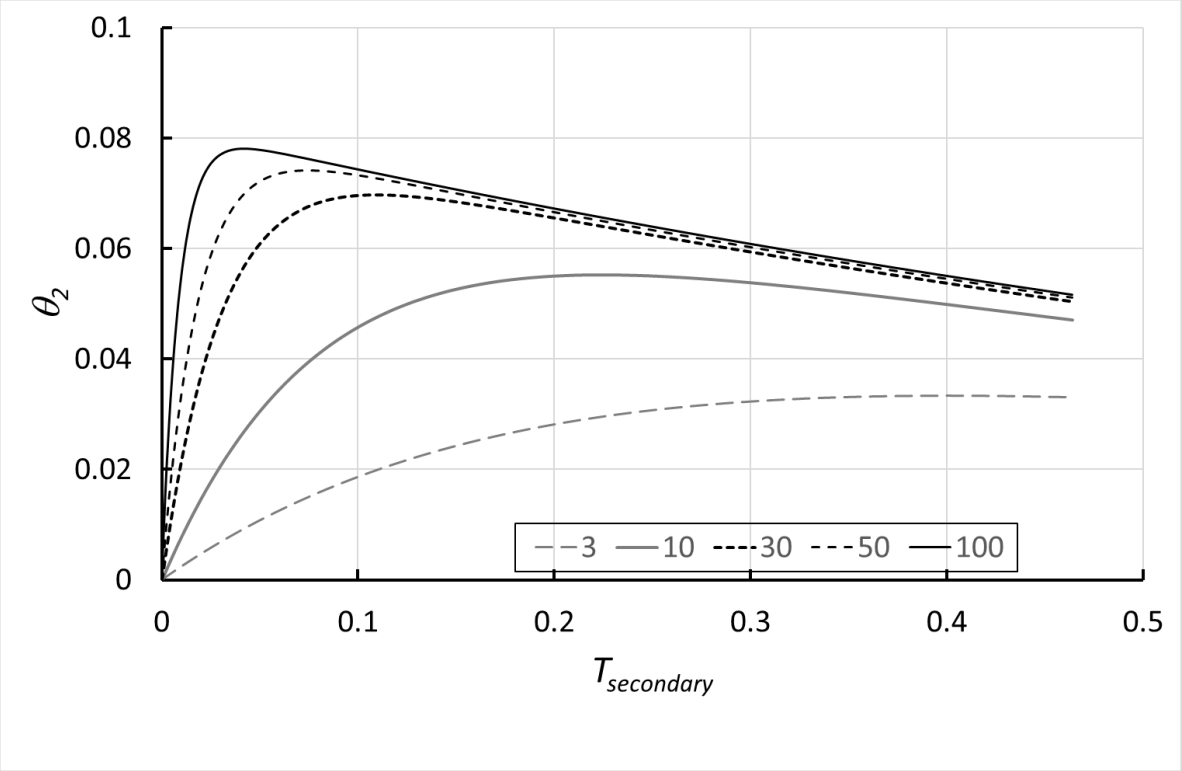

Figure 2. Time variation of the surface coverage of the secondary (indicator) reagent, θ_2 , with different scaled secondary reagent concentration (legend). Scaled analyte concentration, $\Gamma = 1$; primary incubation time, $T_{primary}$ = 0.1, scaled 'off' rate, K_{off} = 1 . The decay at longer time is a consequence of the dissociation from the surface of the bound target analyte and of the secondary reagent from the bound target.

The principal determinant of the assay sensitivity and dynamic range is the amount of analyte captured in the primary incubation step, θ_1 . If K_{off} is small, then equation (9) has solution:

$$\theta_1 = \frac{\Gamma(1-\exp(-T(1-\Gamma))}{(1-\Gamma\exp(-T(1-\Gamma))} \qquad \Gamma \neq 1 \tag{13}$$

So if $T(1-\Gamma)$ is small : $\theta_1 = \Gamma T$.

And can be approximated to second order:

$$\theta_1 \approx \frac{\Gamma T}{\frac{1}{1-(T(1-\Gamma)/2)} + \Gamma T} \approx \frac{\Gamma T}{1+\Gamma T} \tag{14}$$

That is, the assay will noticeably deviate from linearity when ΓT is large enough, say $\Gamma T \sim 0.1$. Figure 3 shows a numerical solution example compared with equations (13) and (14). Equation (14) is a useful approximation for fitting the assay data and thereby extending the dynamic range.

The assay can be tuned for sensitivity and dynamic range by altering the scaling factors for time, $\tau = V/(k_{on}N_A)$ and concentration, N_A/V , which is conveniently done by altering the sample volume, V, and loading of the capture species on the capture bead, N_A. .

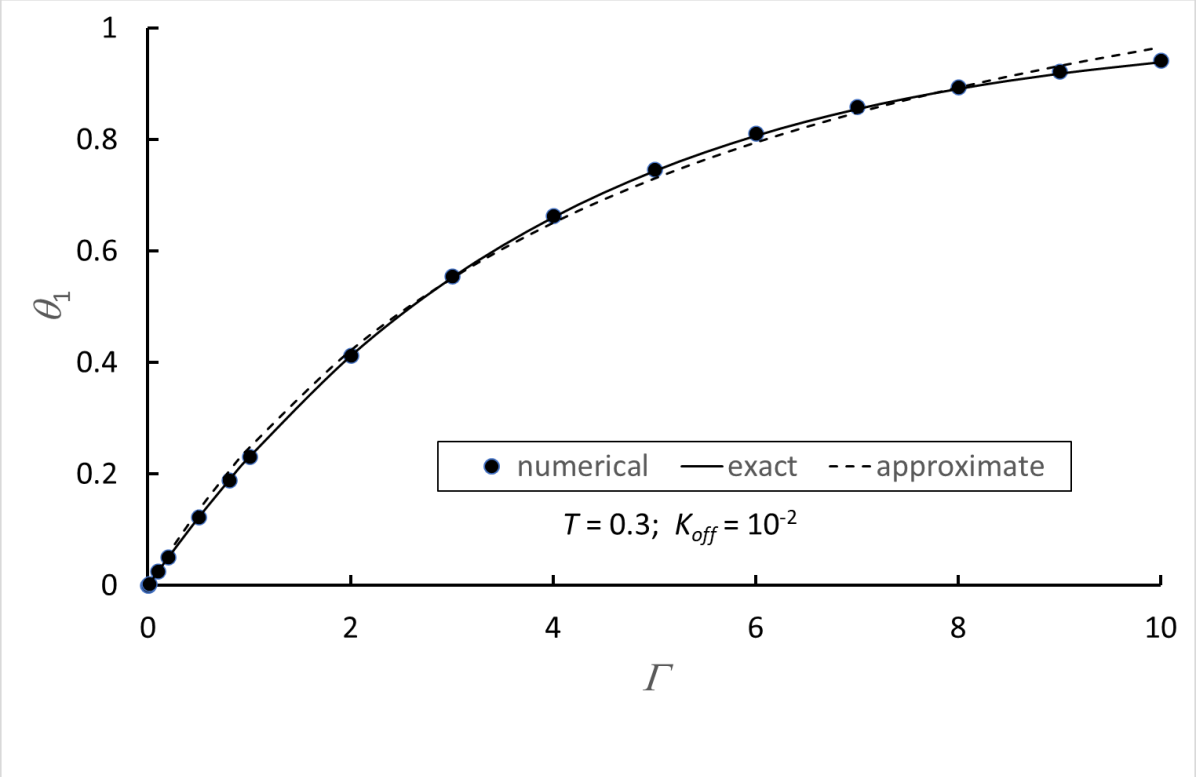

Figure 3. Numerical solution of equation (9) compared with equations (13) (labelled 'exact') and (14) (labelled 'approximate').

Signal generation

The assay is an implementation of a standard Enzyme-Linked Immunosorbent Assay (ELISA) with colorimetric output. There are 5 steps:

a) Capture of the antibody to be measured onto a surface carrying the antigen specific for the antibody. For the SARS-CoV-2 assay, the antigen is the Receptor Binding Domain (RBD) protein. (SARS-CoV-2 (2019-nCoV) Spike RBD-His Recombinant Protein, Biotinylated -Sino Biologicals 40592-V08H-B)
b) Washing off all unbound material
c) Incubation of the capture surface with horseradish peroxidase (HRP) – labelled anti-human IgG (Goat anti-Human IgG Fc Secondary Antibody HRP - Thermofisher - A18817)
d) Washing off unbound material
e) Incubation with a solution of tetramethyl benzidine and hydrogen peroxide (TMB) and measurement of the variation over time of the blue colour that is developed.

The control antibody is SARS-CoV-2 Spike Protein (S-ECD/RBD) Monoclonal Antibody (bcb01) - Thermofisher - MA5-35948

The key to the assay accuracy is rapid and complete mixing and rapid timing. The assay result is controlled by the kinetics of binding in steps a) and c) and the speed of washing in steps b) and d). With these fixed and under control, the development of colour in step e), determined by the amount of HRP bound onto the surface, can reliably be related back to the concentration of antibody present in the sample solution. The objective is to determine, from the time dependence of the result, the rate constant for colour development relative to that for a control sample of known concentration.

a) <u>Expected time-dependence of assay signal</u>

The assumption is that the concentration of hydrogen peroxide is sufficiently high that it does not influence the rate of conversion of colourless TMB to its blue-coloured product. Letting c_{TMB1} denote the concentration of the blue product (concentration at the start of the incubation is zero and at the end is equal to the concentration of colourless TMB added, denoted c_{TMB}), the conversion is assumed to be a first-order chemical reaction with rate constant proportional to the concentration of HRP that is present.

$$c_{TMB1} = c_{TMB}\big(1 - exp(-kt)\big) \tag{15}$$

Where t is the elapsed time since addition of TMB and k is the rate constant. Letting $k_{control}$ and $c_{control}$ denote respectively the rate constant determined for the control sample and the concentration of the control sample, then the concentration of the unknown sample, $c_{unknown}$, with measured rate constant $k_{unknown}$ is:

$$c_{unknown} = c_{control}\frac{k_{unknown}}{k_{control}} \tag{16}$$

Concentration is measured by measuring the intensity transmitted through the solution of light of wavelength matching the wavelength of maximum absorption of the blue product. The relationship of light intensity to concentration would be given by Beer's law (I denotes measured transmitted light intensity, I_0 the source intensity, L the length of the light path through the solution and ε the absorption coefficient of the blue product:

$$\frac{I}{I_0} = \exp\left(-\varepsilon L c\right) \tag{17}$$

However, if the light path,L, is sufficiently short that the amount of light absorbed is small then a simplifying approximation can be made:

$$\frac{I}{I_0} \approx 1 - \ \varepsilon L c \tag{18}$$

In that case, the variation of light intensity with time would be:

$$\frac{I_0 - I}{I_0 - I_\infty} = (1 - exp(-kt) \tag{19}$$

Where I_0 and I_∞ here denote the light intensity measured at t = 0 (immediately after mixing) and I_∞ is the light intensity at time sufficiently long to convert all the added TMB to its blue product.

b) Confirmation of expected time dependence of signal

Figure 3 shows an assay result for a concentration at the upper end of the required measurement range, where the assay signal – output of a photodiode measuring transmitted light intensity – covers almost the full range. The lines show non-linear least squares fit of the light intensity vs time

assuming a first-order increase with time of concentration of the blue product (eq 15) and either Beer's Law (eq 17) or the linear approximation (eq 18) for the dependence of light intensity on concentration. The fit is reasonable. The rate constant for generation of the blue colour relates directly to the amount of bound secondary indicator (HRP), $\theta_{2,final}N_A$ which relates to the amount of target captured in the primary incubation step and hence to the target analyte concentration.

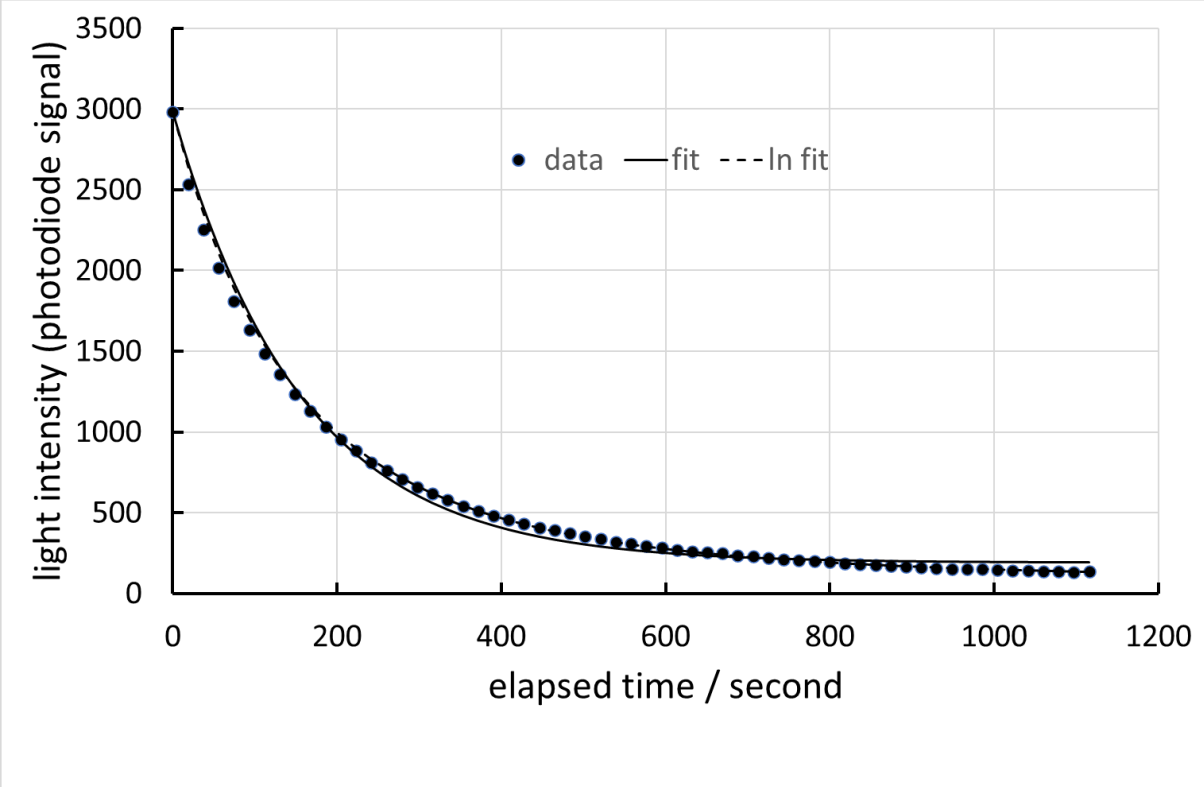

Figure 3 Measured light intensity vs elapsed time from addition of TMB (points) and fit to expected first-order variation assuming Beer's Law (dashed line) and the linear approximation (full line). Analyte concentration 10μg / mL

c) Confirmation of expected dependence of rate constant for signal generation on target concentration and demonstration of wide dynamic range.

Figure 4(a) shows assay signal development with different concentration of target in the diluted solution. The rate constant for signal development increases smoothly with increasing target concentration. Figure 4(b) illustrates the performance of a fitting algorithm designed to progress smoothly from the linear variation at low analyte concentration to the exponential variation at high analyte concentration (equation 19). The desired result is the initial slope relative to that for a control on the same disc (equation 16). Figure 5 shows the variation of derived rate constant with target analyte concentration. The variation is consistent with the approximate solution, equation (14). Saturation of the signal is caused by saturation of the capture surface ($\theta_1 \rightarrow 1$). The dynamic range is over a scale of about 200 times in concentration. The linear range is over a range of approximately 20 times in concentration. As noted above, the assay range can be adjusted primarily by altering the loading of the capture antigen onto the capture surface. The difference between duplicate measurements is 10% of the measurement across the assay range and would be largely

determined by the timing accuracy. The assay is sufficiently sensitive that the sample can be heavily diluted with buffer, which is helpful in normalising samples as variable as blood.

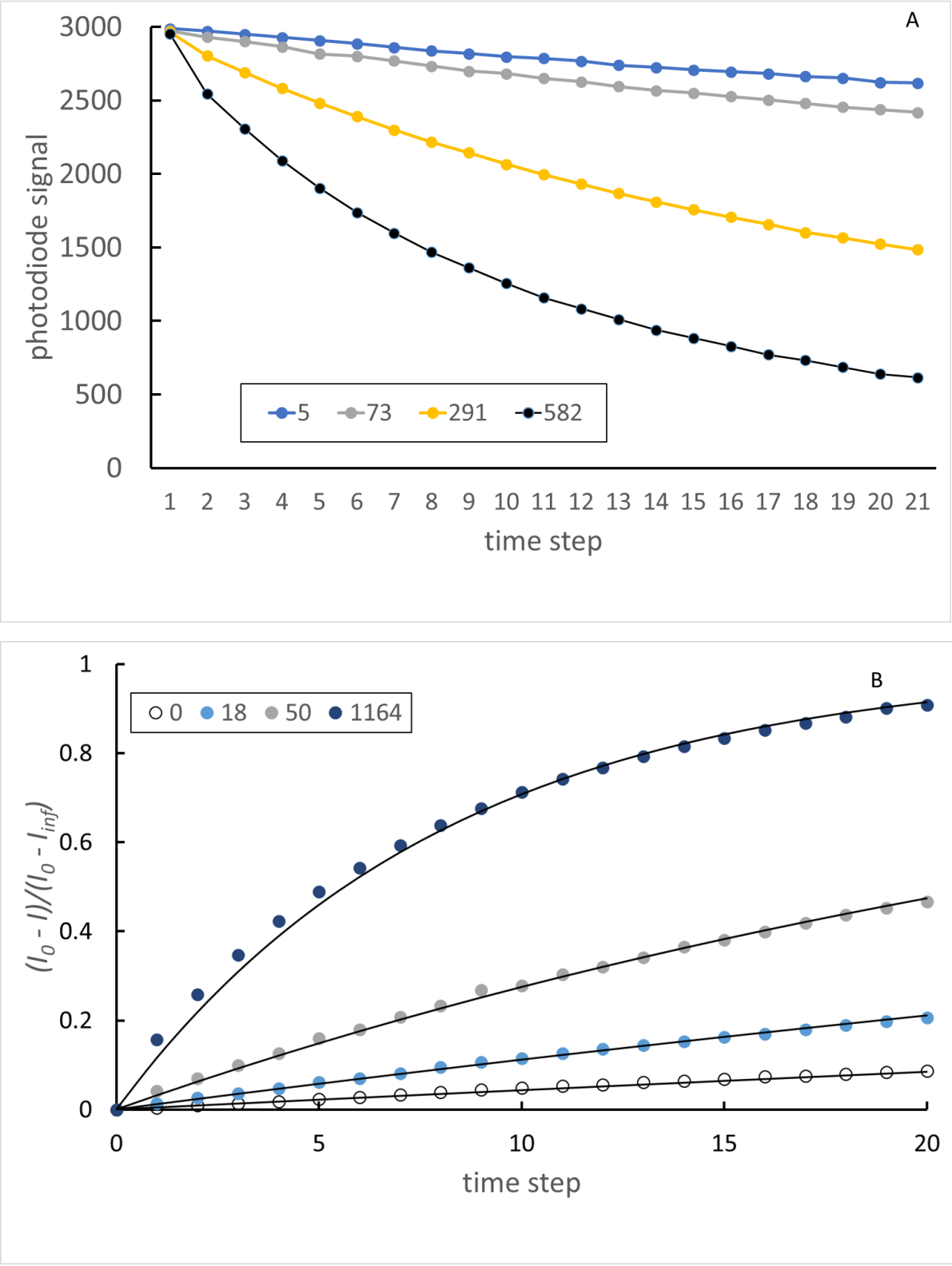

Figure 4. A: Variation of colour development with change of target analyte concentration. The rate constant is extracted as the assay signal. Legend: diluted target concentration, ng / mL. The time step is 18 s. B: Variation according to equation (19) Lines are fitted with an algorithm designed to

move smoothly from the linear regime at low analyte concentration to the exponential regime at high concentration

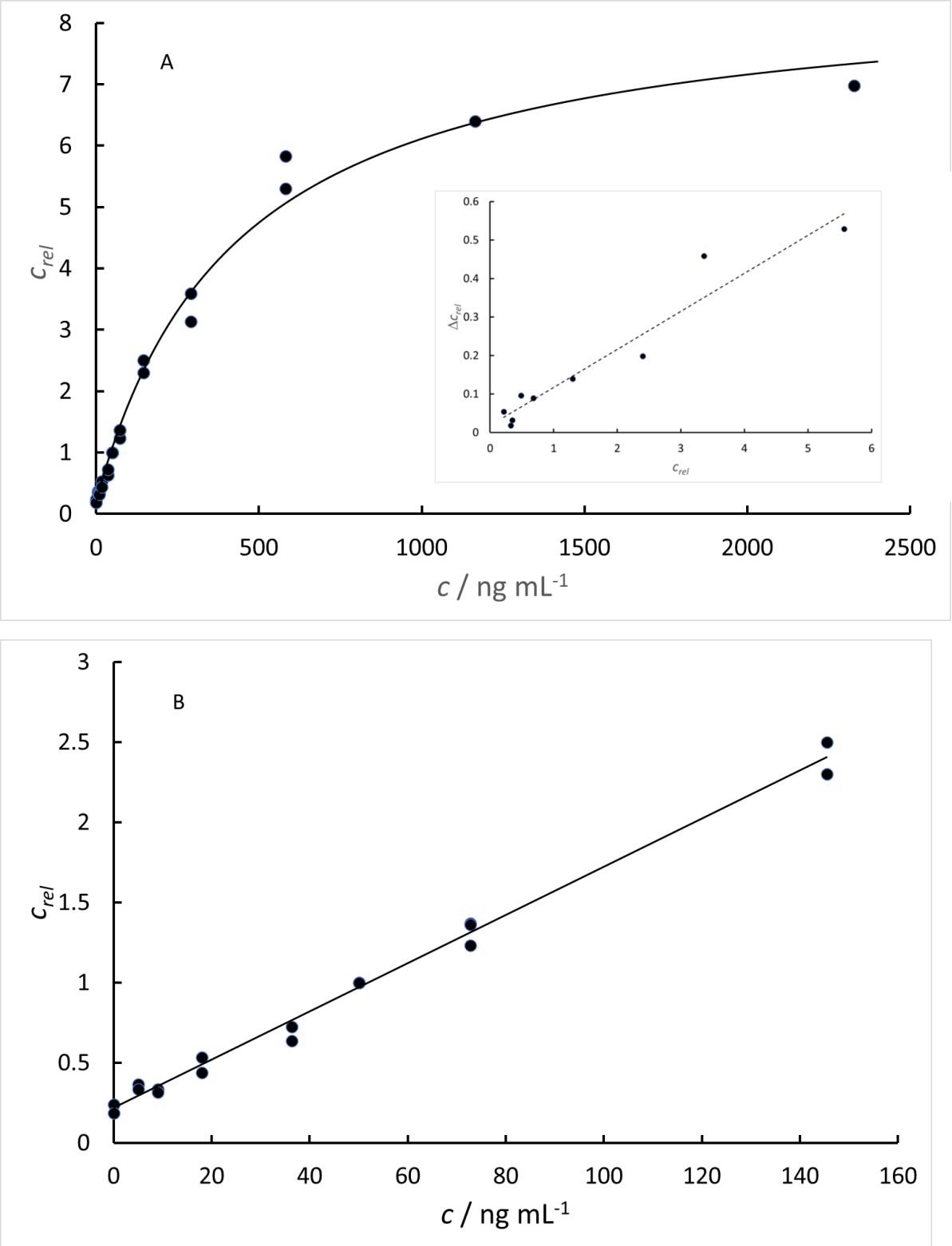

Figure 5. A. Variation of rate constant for colour development relative to the control (50 ng / mL). The line is a fit to the approximate solution of eq (14). Inset: Difference between duplicate measurements relative to the control, Δc_{rel} as a function of the measured concentration

relative to the control, c_{rel} ; the assay shows a coefficient of variation of 10% that is essentially constant across the assay range. B: linear range at low target analyte concentration; concentration relative to the control, c_{rel}, against sample concentration, c.

Supplementary Appendix 2

Individual vaccine efficacy variation with time since mRNA BNT162b2 vaccination estimated by rapid, quantitative antibody measurements from a finger-prick sample.

Matheus J. T. Vargas, Mithileshwari Chandrasekhar, Yong Je Kwon, Gerrit Sjoerd Deijs, Carsten Ma On Wong Corazza, Angela (Wai Yin) Chai, Rebecca L. Binedell, Ellen Jose, Bhavesh Govind, Laura Huyet, Pooja K. Patel, Gabrielle Reshef, Vijaya Kumar, Tiffany Lowe, Flynn C.W. Walker, Apisalome Talemaitoga, MD, M. Cather Simpson, David E. Williams*

Assay validation with WHO standards

Panel 20/770 from the National Institute for Biological Standards and Control, UK, (NIBSC) comprises a set of plasma samples from convalescent Covid-19 patients as well as a set of pre-Covid negative samples. With the panel is provided a set of analytical results performed on a variety of different medical laboratory assay platforms. Because all the platforms have a different concentration scale, for the comparisons below, these results have been scaled to the median for the set, determined for each platform. The in-house assay from Public Health England, Colindale Laboratory, is taken as the comparator. Figure 1 shows the correlation of the various assays with the PHE Colindale result.

Figure 2 shows the correlation of the Orbis assay result with PHE, including a direct comparison with the Abbott result. On the Orbis assay, the negative plasma samples showed the same non-specific binding offset observed for the clinical study negatives, with closely similar mean and standard deviation. The mean offset was therefore subtracted from the assay result. Orbis and Abbott show similar correlation, with a correlation slope close to unity.

The Euroimmun and Ortho assays correlate well with PHE Colindale. The correlation of Abbot and Diapro with PHE Colindale is similar to that of the Orbis assay at its current state of development. The correlation of the data given for the Roche Elecsys with that for these other assay systems is poor. We have established by sample dilution that the Roche assay results given in the package insert for this panel show a very significant high-dose hook effect[1].

The difference in results for the different assays can probably be related to differences in assay design and capture reagent, in response to samples containing a range of antibodies of different affinity for the chosen target. Plate-based assays are usually incubated to equilibrium (at least 1 hr) and therefore develop results reflecting the antibody affinity. In contrast, the Orbis assay is designed for speed to result, with incubation time 5 minutes. The result is determined by the 'on' rate for the antibody, which may not be the same for antibodies of the same affinity. Laboratory systems like the Abbott Architect use incubation times of ~ 20 min and therefore have result determined both by affinity and 'on' rate.

[1] Measurement kindly performed by C.J Pemberton, Christchurch Heart Institute, Department of Medicine, University of Otago, Christchurch

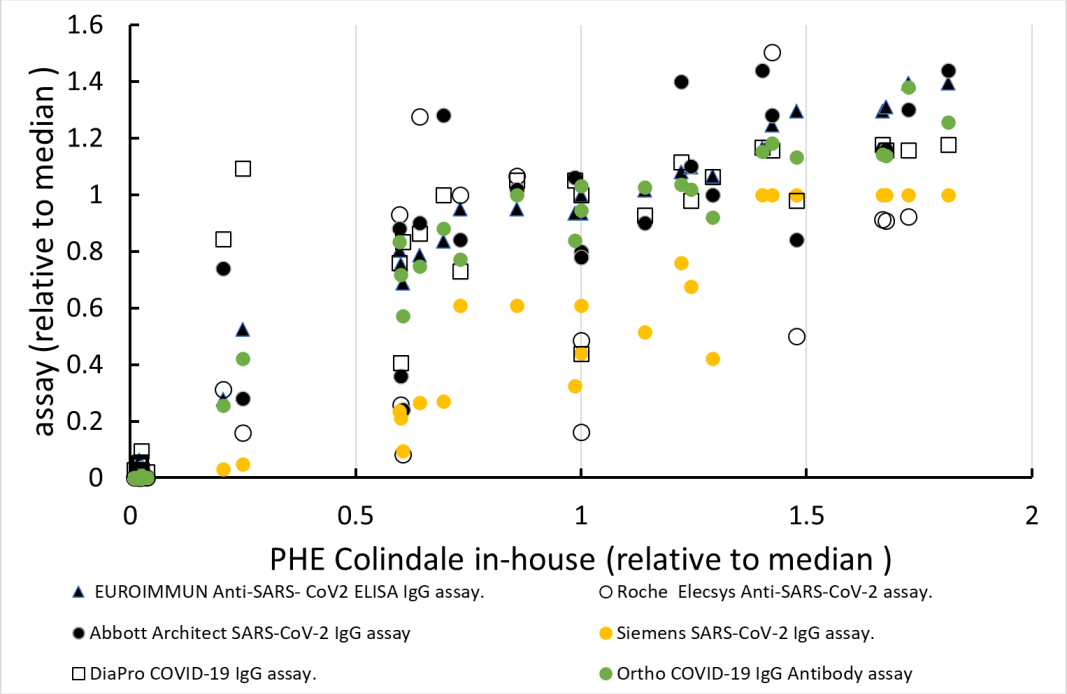

Figure 1. Correlation of results from different medical laboratory immunoassay platforms for the NIBSC 20/B770 panel, taking the PHE Colindale assay as the comparator; data from the 20/B770 package insert.

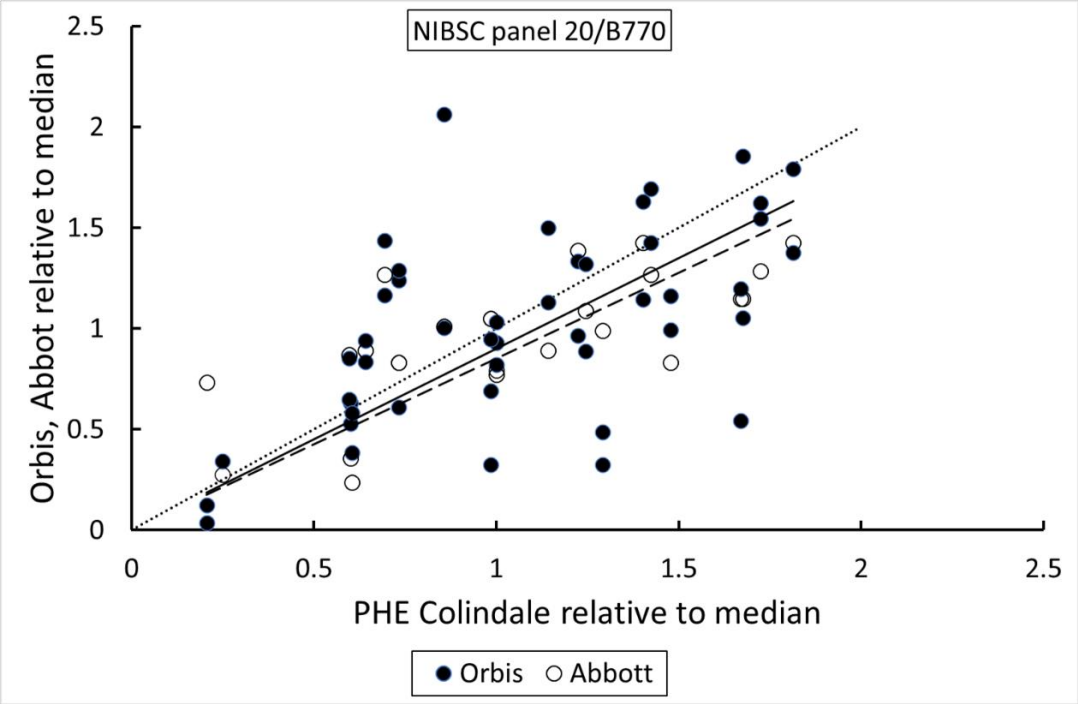

Figure 2 Correlation of Orbis assay result (sample / control, non-specific binding offset corrected) with the result for PHE Colindale for panel 20/B770; Comparison with Abbott result from the 20/B770 package insert. The lines are: dotted – 1:1 correlation; solid- Orbis, R^2 = 0.87; dashed – Abbott, R^2 = 0.92.

In order to express the Orbis assay results on a recognised comparison scale, the standard reagents NIBSC 20/162 and the panel 20/150 were measured. Figure 3 shows the result.

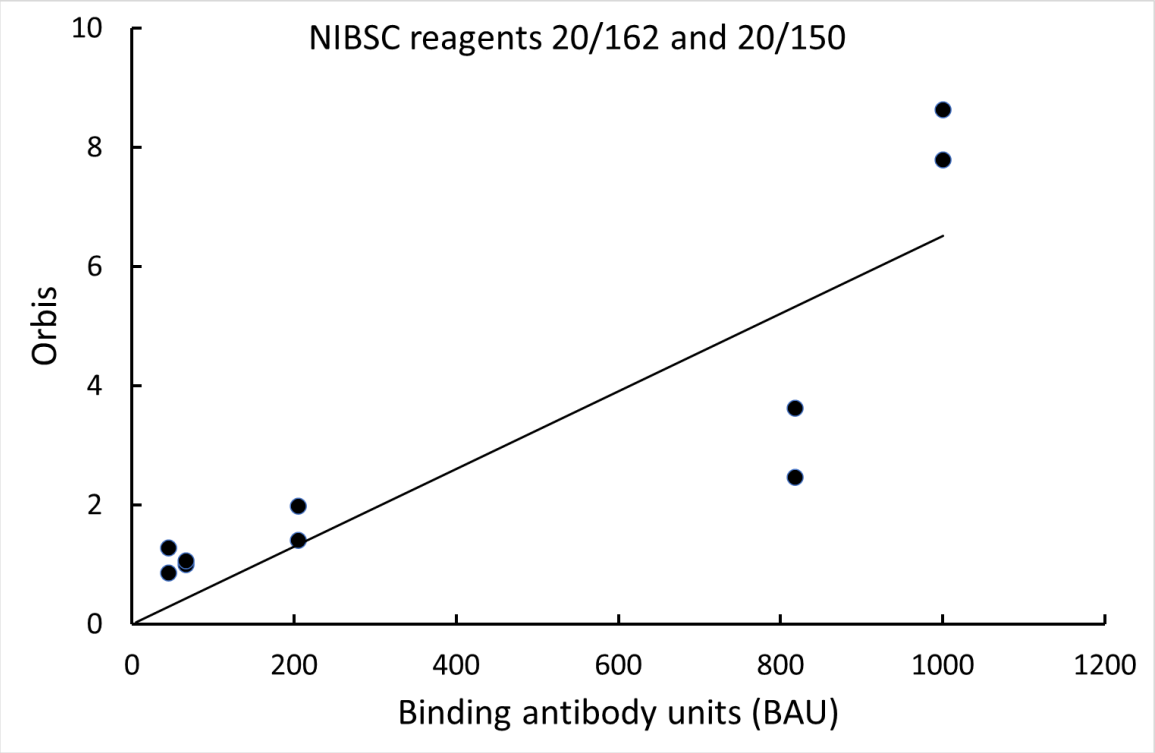

Figure 3. Orbis assay (non-specific binding offset corrected) results for WHO standard samples

The NIBSC gives concentration of anti-receptor binding domain IgG in 'binding antibody unit' (BAU) derived for each sample as the median (geometric mean) of the results from a number of different assay methods. The samples, being derived from convalescent plasma, would contain antibodies with a range of different binding affinity that may react differently in different assays dependent on the details of the assay design. The range of antibodies present would be different in each sample. Exact agreement is not therefore to be expected.

Supplementary Appendix 3

Individual vaccine efficacy variation with time since mRNA BNT162b2 vaccination estimated by

Matheus J. T. Vargas, Mithileshwari Chandrasekhar, Yong Je Kwon, Gerrit Sjoerd Deijs, Carsten Ma On Wong Corazza, Angela (Wai Yin) Chai, Rebecca L. Binedell, Ellen Jose, Bhavesh Govind, Laura Huyet, Pooja K. Patel, Gabrielle Reshef, Vijaya Kumar, Tiffany Lowe, Flynn C.W. Walker, Apisalome Talemaitoga, MD, M. Cather Simpson, David E. Williams*

Estimating individual vaccine efficacy from population breakthrough risk

1. Vaccine efficacy model for an individual.
2. Breakthrough infection risk by integrating across population antibody concentration distribution.
3. Vaccine efficacy data over time since vaccination from Tartof et al. [1]
4. Use of distributions over different date ranges to derive parameters of vaccine efficacy model
5. Reasonableness of parameters.

1. Vaccine efficacy model for an individual

Khouri et al.[2] have described empirically the dependence of vaccine protective efficacy on neutralising antibody concentration. Williams has shown how the observed dependence has a simple physical explanation in the statistics of binding of antibody to the viral spikes [3]. Therefore it is reasonable to use this model to relate the concentration of anti-receptor binding domain (RBD) IgG to vaccine efficacy, perhaps with parameters slightly different to those derived by Khouri but which should be consistent with the model developed by Williams.

The model is:

$$E_I(c) = 1/[1 + (c_{50}/c)^k] \quad (1)$$

Where $E_I(c)$ denotes vaccine protective efficacy as a function of concentration, c, of anti RBD IgG. The curve is a sigmoidal variation of ln(c). The parameters are c_{50} and k where c_{50} denotes the concentration for 50% vaccine efficacy and k controls the rate of increase of efficacy with concentration around c_{50} . In what follows, c_{50} and k will be adjusted to match observed results for population breakthrough infection.

2. Breakthrough infection risk by integrating across population antibody concentration distribution

Williams [4] used equation (1) to derive population breakthrough risk given a known antibody concentration distribution across the population.

$$P(protected) = \int_0^\infty E_I(c) f_V(c) dc \quad (2)$$

Where $f_V(c)$ denotes the probability density of concentration, *c*, across the population. As demonstrated, this distribution is log-normal, consistent with the observations of Khouri et al.

$$f_V(c) \sim \mathbb{N}(\ln(c)|\mu,\sigma) \tag{3}$$

Where the mean, μ, and standard deviation, σ, may vary with time since vaccination.

Therefore, if there are sufficient data to estimate the mean, μ, and standard deviation, σ, over a range of time since vaccination, then an estimate of vaccine efficacy, *VE*, over this time range can be obtained:

$$VE = P(protected) = \int_0^\infty \left(1/[1+(c_{50}/c)^k]\right)\mathbb{N}(\ln(c)|\mu,\sigma)dc \tag{4}$$

If the vaccine efficacy over this time range is known from population infection statistics comparing vaccinated and unvaccinated people, then if data for enough time ranges is available the parameters c_{50} and *k* may be adjusted to obtain agreement between observed and computed efficacy. The functions and integral can be evaluated in a Microsoft Excel spreadsheet. The unknown parameters c_{50} and *k* can be estimated by optimising the match between observed and calculated VE for the different time ranges for which data are available, with adjustment of the parameters μ and σ to obtain consistency between the distribution of vaccine efficacy calculated for the samples from equation (1) and the assessment of distribution of antibody concentration derived from fitting the measurements for the samples, represented by equation (3).

3. Vaccine efficacy data over time since vaccination, from Tartof et al. [1]

Tartof et al obtained vaccine efficacy against infection for the Pfizer-BioNtech vaccine varying with time since vaccination using data scoured from medical records of over 3M people. Results averaged across all variants are given in Table 1

Table 1

Vaccine efficacy against symptomatic infection, un-adjusted for age. ethnicity and other factors[1]					
< 1 month	1 to <2	2 to <3	3 to <4	4 to <5	>=5
88 (86-89)	83 (81-85)	77 (78-79)	68 (65-70)	61 (58-64)	47 (43-51)

4. Use of distributions over different date ranges to derive parameters of vaccine efficacy model

Figure 1 shows the distribution of time since second dose across the clinical study participants. Data fall into 3 distinct time range groups : < 90 days; 90 - 170 days and 170 – 228 days (the maximum value in the study). For each of these ranges a weighted average efficacy was calculated from Table 1. Log-normal mean and standard deviation of anti-RBD IgG concentration was calculated for each time range. Given these values, the integral of equation (4) was evaluated for each time range and the parameters c_{50} and *k* adjusted to minimise the squared deviations of calculated and observed VE across the three time ranges. However, if these parameters were then used to calculate VE from the measured study antibody concentration data, using equation (1), the distribution of VE obtained differed greatly from that calculated using the theoretical distribution fitted according to equation

(3), as shown in figure 2. The fitted results are given in table 2. The value of *k* is outside the confidence range given by Khouri et al. An alternative procedure was adopted: by empirical search to find a solution that approximated both the observed concentration distribution and calculated vaccine efficacy distribution, under the constraint that the log-normal standard deviation of concentration was the same for all three time ranges, and that reasonably approximated the observed population vaccine efficacy from Tartof et al. Figure 3 and Table 3 show the results, which are reproduced in the main text.

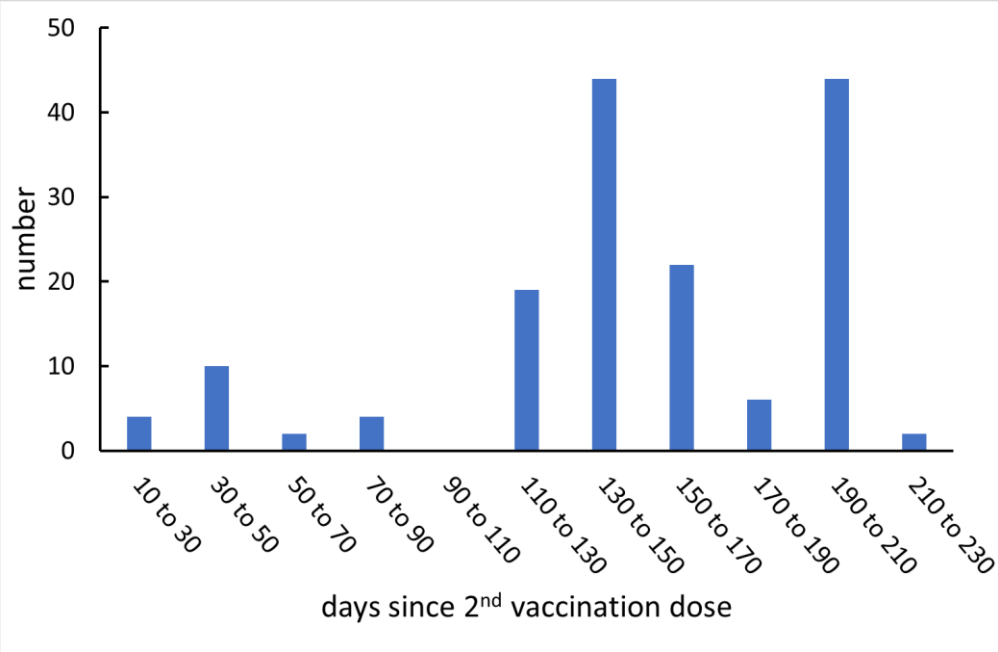

Figure 1: Distribution of number of study participants across days since second vaccine dose.

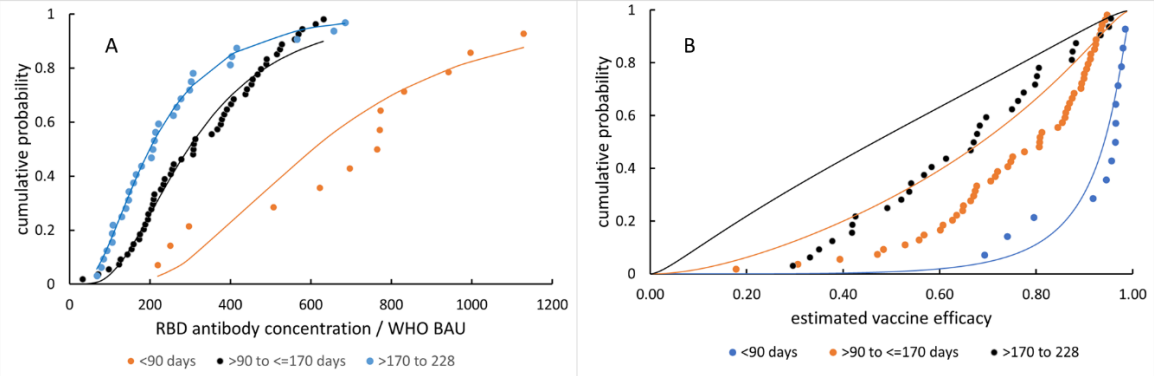

Figure 2. Vaccine efficacy estimation by first obtaining best fit log-normal cumulative distribution to observed empirical cumulative distribution of concentration (A); then adjusting c_{50} and *k* in equation (4) to match the observed vaccine efficacy (B). The lines in (B) are the distribution of vaccine efficacy across the population using the fitted concentration distribution; the points use the measured concentration.

Table 2. Observed and calculated (equation (4) vaccine efficacy. The parameters μ and σ are first fitted to the observed cumulative distributions. Then the parameters c_{50} and *k*. are fitted to observed vaccine efficacy

Time range / days	< 90	90 - 170	170 - 228

μ	1.62	0.78	0.39
σ	0.48	0.60	0.68
VE(observed: Tartof)	83	64	47
VE(calculated)	83	63	47
C_{50} / BAU	211		
k	2.37		

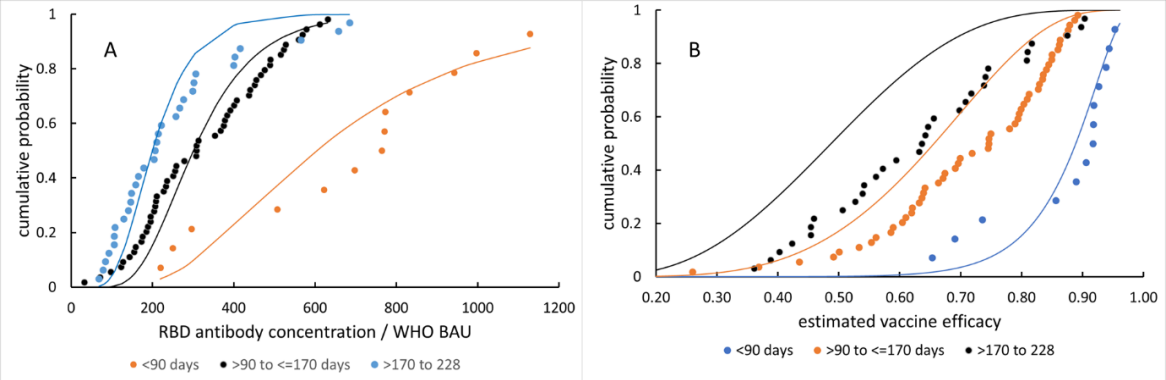

Figure 3. Vaccine efficacy estimation by empirical search. The log-normal standard deviation σ is constrained to be the same for all time ranges. The log-normal mean, μ, is a fitting parameter different for each time range. The parameters σ, μ, c_{50} and k (eq 3 and 4) are adjusted by empirical search to match the observed concentration distribution, deduced vaccine efficacy distribution and observed population vaccine efficacy. (A): the concentration cumulative distribution; points: the measured empirical cumulative distribution; lines: cumulative distribution corresponding to equation (3). (B) the deduced vaccine efficacy distribution; points: empirical cumulative distribution using measured concentrations and equation (1); lines: cumulative distribution using equation (1) and the fitted concentration distribution, equation (3). .

Table 3. Observed and calculated (equation (4) vaccine efficacy. The parameter σ is constrained to be the same for all time ranges. Then the parameters σ, μ, c_{50} and k. are adjusted by empirical search to match the observed concentration distribution, deduced vaccine efficacy distribution and observed population vaccine efficacy

Time range / days	< 90	90 - 170	170 - 228
μ	1.62	0.78	0.39
σ	0.4		
Population VE(observed: Tartof)/ %	83	64	47
Population VE(calculated)	82	64	49
C_{50} / BAU	206		
k	1.70		

5. Reasonableness of parameters.

The estimate of k is not dependent on the antibody concentration units used. Khouri et al give k = 1.30 with 95% confidence interval 0.96 – 1.82. Williams has shown that this range is consistent with a simple physical model for antibody protection. The estimated k is very consistent with this value. Determination of c_{50} is dependent on the concentration scale used. In order to avoid this difficulty, Khouri et al gave the values as a multiple of the median convalescent antibody concentration, z_{50} =

0.2 (0.14,0.28). The convalescent median assessed from the 23 samples in the NIBSC 20/B770 panel by the Orbis device is 370 BAU. The Khouri et al. result would thus give c_{50} =74 (51, 103) . The estimated c_{50} is higher. The Khouri et al. result was estimated for the original (Wuhan) variant. The data used here from Tartof et al are an average for all variants present in California. Wall et al.[5] have suggested qualitatively that c_{50} for the Delta variant could be a factor of 6 times higher, implying c_{50} ~ 440 BAU. The estimated c_{50} is indeed consistent with this number, given the range of variants present in the study population of Tartof et al.

1. Tartof, S. Y.; Slezak, J. M.; Fischer, H.; Hong, V.; Ackerson, B. K.; Ranasinghe, O. N.; Frankland, T. B.; Ogun, O. A.; Zamparo, J. M.; Gray, S.; Valluri, S. R.; Pan, K.; Angulo, F. J.; Jodar, L.; McLaughlin, J. M., Effectiveness of mRNA BNT162b2 COVID-19 vaccine up to 6 months in a large integrated health system in the USA: a retrospective cohort study. *The Lancet* **2021,** *398* (10309), 1407-1416.
2. Khoury, D. S.; Cromer, D.; Reynaldi, A.; Schlub, T. E.; Wheatley, A. K.; Juno, J. A.; Subbarao, K.; Kent, S. J.; Triccas, J. A.; Davenport, M. P., Neutralizing antibody levels are highly predictive of immune protection from symptomatic SARS-CoV-2 infection. *Nature Medicine* **2021,** *27* (7), 1205-1211.
3. Williams, D. E., COVID 19 breakthrough infection risk: a simple physical model describing the dependence on antibody concentration. *bioRxiv* **2021**, 2021.10.25.465798.
4. Williams, D. E., Importation Risk Stratification for COVID19 using Quantitative Serology. *medRxiv* **2021**, 2021.09.29.21264323.
5. Wall, E. C.; Wu, M.; Harvey, R.; Kelly, G.; Warchal, S.; Sawyer, C.; Daniels, R.; Hobson, P.; Hatipoglu, E.; Ngai, Y.; Hussain, S.; Nicod, J.; Goldstone, R.; Ambrose, K.; Hindmarsh, S.; Beale, R.; Riddell, A.; Gamblin, S.; Howell, M.; Kassiotis, G.; Libri, V.; Williams, B.; Swanton, C.; Gandhi, S.; Bauer, D. L. V., Neutralising antibody activity against SARS-CoV-2 VOCs B.1.617.2 and B.1.351 by BNT162b2 vaccination. *Lancet* **2021,** *397* (10292), 2331-2333.